

# Switchable and tunable Rashba-type spin splitting in covalent perovskite oxides

Julien Varignon,<sup>1</sup> Jacobo Santamaria,<sup>2,1</sup> and Manuel Bibes<sup>1</sup>

<sup>1</sup>*Unité Mixte de Physique, CNRS, Thales, Université Paris Sud, Université Paris-Saclay, 91767, Palaiseau, France\**

<sup>2</sup>*Laboratorio de Heteroestructuras con aplicación en Spintronica, Unidad Asociada CSIC/Universidad Complutense de Madrid,*

*Sor Juana Inés de la Cruz, 3, 28049 Madrid, Spain, Instituto de Magnetismo Aplicado, Universidad Complutense de Madrid, 28040 Madrid Spain*

(Dated: August 10, 2018)

In transition metal perovskites ( $\text{ABO}_3$ ) most physical properties are tunable by structural parameters such as the rotation of the  $\text{BO}_6$  octahedra. Examples include the Néel temperature of orthoferrites, the conductivity of mixed-valence manganites, or the band gap of rare-earth scandates. Since oxides often host large internal electric dipoles and can accommodate heavy elements, they also emerge as prime candidates to display Rashba spin-orbit coupling, through which charge and spin currents may be efficiently interconverted. However, despite a few experimental reports in  $\text{SrTiO}_3$ -based interface systems, the Rashba interaction has been little studied in these materials, and its interplay with structural distortions remain unknown. In this Letter, we identify a bismuth-based perovskite with a giant, electrically-switchable Rashba interaction whose amplitude can be controlled by both the ferroelectric polarization and the breathing mode of oxygen octahedra. This particular structural parameter arises from the strongly covalent nature of the Bi-O bonds, reminiscent of the situation in perovskite nickelates. Our results not only provide novel strategies to craft agile spin-charge converters but also highlight the relevance of covalence as a powerful handle to design emerging properties in complex oxides.

Spintronics exploits the spin degree of freedom of carriers in addition to their charge, giving rise to a very broad range of electronic applications including magnetic memories or magnetic sensors [1, 2]. It relies on the exchange interaction of electrons with local magnetic moments of a ferromagnet to generate spin currents. Usually, the ferromagnets are simple transition metal elements such as Co, Ni or their alloys. Nevertheless, the control of their magnetization typically requires large energies and they generate undesired magnetic fields hindering high densification of devices. In the search for lower power spintronic devices, the spin-orbit interaction (SOI) has been identified as a promising pathway to achieve very efficient spin-to-charge current conversion and *vice versa*. The two phenomena at the core of this branch of spintronics, also called spin-orbitronics, are the spin Hall effect (SHE) [3, 4] and inverse spin Hall effect (ISHE) [5, 6]. For instance, the former effect allows efficient charge-to-spin current conversion in non-magnetic materials based on heavy elements [7], therefore alleviating the need for ferromagnets to generate spin currents.

More recently, renewed interest for SOI based applications arise thanks to the Rashba effect [8]. In materials lacking inversion symmetry, the interplay between the electric field and the SOI lifts the degeneracy of electronic bands according to their spin. For a material exhibiting a polar axis oriented along the  $z$  direction, Rashba proposed the following spin-orbit interaction:

$$H_R = \alpha_R(\sigma_x k_y - \sigma_y k_x) \quad (1)$$

where  $\alpha_R$  is the Rashba coefficient – proportional to the spin-orbit strength of the material  $\lambda_{\text{SO}}$  and to the magni-

tude of the electric field –,  $\sigma_i$  ( $i=x,y$ ) are Pauli matrices and  $k_j$  ( $j=x,y$ ) is the momentum of the electron. The Rashba interaction leads to a spin-locking of electrons according to their momentum  $\vec{k}$  enabling efficient spin-to-charge current interconversions through Edelstein and inverse Edelstein effects [9, 10]. Although originally formulated at interfaces and surfaces [11–14], the Rashba interaction is now generalized to non-centrosymmetric bulk materials [15–17], although it may coexist with the Dresselhaus interaction [18].

In the context of SOI related devices,  $\text{ABO}_3$  oxide perovskites remain largely unexplored. They encompass a wealth of properties – including ferroelectricity and magnetism – and functionalities originating from the coupling of their structural, electronic and magnetic degrees of freedom [19]. Most notably, the lattice distortions usually control the properties of the perovskite, such as the metal-insulator phase transition temperature in rare-earth nickelates [20, 21], the Néel temperature of orthoferrites [22, 23] or the band gap value of rare-earth scandates [24, 25]. Being largely ionic in most cases, many oxide perovskites host large internal electric dipoles. Moreover, they can also accommodate heavy elements, an important aspect for SOI based applications. So far,  $\text{BiAlO}_3$  has been proposed theoretically to be the first oxide exhibiting ferroelectricity and Rashba physics [17] – although this coexistence was already observed in the semiconductor  $\text{GeTe}$  [16]. While  $\text{BiAlO}_3$  harbors a heavy element and a large ferroelectric polarization – estimated around  $90 \mu\text{C.cm}^{-2}$  –, the computed Rashba coefficient  $\alpha_R$  remains relatively moderate – around 0.39 and 0.74 eV.Å – although comparable to conventional systems such

as (111) oriented Bi [26]. In fact, other ingredients such as a narrow band gap and/or similar atomic and orbital characters for the electronic states located around the Fermi level are proposed to be additional key ingredients for reaching large  $\alpha_R$  [27]. Covalent oxides that are characterized by a strong hybridization of B cations and O anions electronic states around the Fermi level, are therefore an ideal platform to engineer materials undergoing large Rashba effects. Furthermore, oxides are usually characterized by numerous lattice distortions but the role of the latter on the Rashba physics remains unexplored.

In this letter, we use *first-principles* simulations to identify the existence of large Rashba effects with  $\alpha_R$  as large as 8 eV.Å in a ferroelectric phase of the covalent oxide strontium bismuthate SrBiO<sub>3</sub> reachable by epitaxial strain. We further reveal that the amplitude of the Rashba coefficient is tunable by a lattice distortion strongly connected to bands dispersion and to the level of hybridization between B and O electronic states. Our results therefore highlight a new pathway to control and optimize the Rashba interaction in oxides, further revealing the potential of these materials for spin-orbitronics.

Strontium bismuthate Sr<sup>2+</sup>Bi<sup>4+</sup>O<sub>3</sub> is an insulator adopting a monoclinic  $P2_1/n$  symmetry at low temperature [28, 29]. The ground state structure is characterized by the usual oxygen cage rotations appearing in perovskites,  $a^-a^-c^+$  antiferrodistortive motions in Glazer's notation, as well as by a breathing of the oxygen cage octahedra distortion  $B_{oc}$  (see Figure 1.a) [28, 29]. The latter distortion produces a rocksalt-like pattern of large and small O<sub>6</sub> groups resulting in Bi sites splitting. In the following, Bi cations sitting in compressed (extended) O<sub>6</sub> groups are labeled Bi<sub>S</sub> (Bi<sub>L</sub>) (see Figure 1.a). Since SrBiO<sub>3</sub> shares several features with rare-earth nickelates RNiO<sub>3</sub>, the appearance of  $B_{oc}$  in bismuthates is sometimes interpreted in terms of ionic charge disproportionation of unstable Bi<sup>4+</sup> valence state to the more stable Bi<sub>L</sub><sup>3+</sup> + Bi<sub>S</sub><sup>3+</sup> electronic configurations in the insulating phase [30–32]. Alternatively, it is also proposed to be a consequence of charge transfer effects from O anions to Bi cations [33]. Nevertheless, Tonnhauser and Rabe demonstrated that the appearance of  $B_{oc}$  is responsible of the band gap opening in bismuthates [34].

Although very similar to rare-earth nickelates, bismuthates also exhibit many other striking properties such as high  $T_c$  superconductivity upon hole doping [29, 35–38] or possible topological surface states accessible upon electron doping [39]. The latter point highlights the strength of the SOI in these materials, being *de facto* an ideal playground to study theoretically the interplay between lattice distortions, covalence and spin-orbit related phenomena.

*First-principles* calculations were carried out with Density Functional Theory (DFT) using the Vienna *Ab initio* Simulation Package (VASP) [40, 41]. We used the PBE functional revised for solids [42] with a cutoff en-

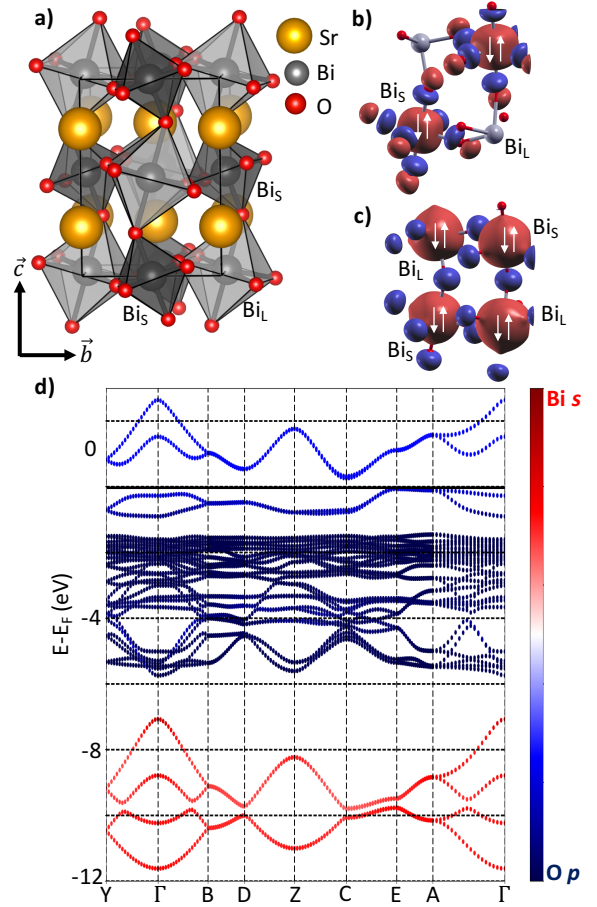


FIG. 1. Structural and electronic properties of SrBiO<sub>3</sub> ground state. a) Ground state  $P2_1/n$  monoclinic structure. b)  $s$ -like Wannier functions associated with the 2 bands lying above the Fermi level. c)  $s$ -like Wannier functions associated with the 4 low lying bands between -12 eV and -6 eV. d) Angular momentum resolved band structure of the monoclinic  $P2_1/n$  phase. The Fermi level  $E_F$  is set to 0. The high symmetry coordinates in the Brillouin zone of the  $P2_1/n$  symmetry are the following:  $\Gamma$  (0,0,0), B (1/2,0,0), Y (0, 1/2,0), A (1/2,1/2,0), Z (0,0,1/2), C (0,1/2,1/2), E(1/2,1/2,1/2) and D(1/2,0,1/2).

ergy of 500 eV and a  $6 \times 6 \times 4$  ( $4 \times 4 \times 4$ ) Monkhorst-Pack kpoint mesh for 20 (40) atoms unit cells. We used Projector Augmented Waves (PAW) pseudopotentials [43] for core electrons with the following valence electron configurations:  $4s^2 4p^6 5s^2$  (Sr),  $6s^2 6p^3$  (Bi) and  $2s^2 2p^4$  (O). Geometry optimizations were performed until forces are lower than 0.01 meV.Å<sup>-1</sup> without spin-orbit interaction included unless stated. Born effective charges and phonons frequencies were computed with the density functional perturbation theory [44, 45]. Band structures and spin textures were plotted with the PyProcar script [46]. Maxi-Localized Wannier Functions (MLWFs) were extracted with the Wannier90 package [47–49].

We first inspect the properties of bulk strontium bismuthate. Geometry relaxation yields an insulating mon-

oclinic  $P2_1/n$  ground state with a band gap of 0.3 eV, other polymorphs observed experimentally at higher temperature –  $Fm\bar{3}m$ ,  $R\bar{3}c$  or  $I_2/m$  symmetries – are found higher in energies. Our optimized lattice parameters ( $a=5.9400$  Å,  $b=6.1365$  Å,  $c=8.4859$  Å and  $\beta=90.0597^\circ$ ) are found in very good agreement with experiments from reference 29, yielding 0.55 % of error on the total volume. Regarding the electronic structure of the material, we extract for both  $\text{Bi}_S$  and  $\text{Bi}_L$  cations similar site occupancies  $N$ , although a weak charge order does exist but with a sign opposite to that expected ( $N_{\text{Bi}_S}=3.97e$  while  $N_{\text{Bi}_L}=3.55e$ ). The quasi-absence of charge ordering can be further appreciated on the projected band structure on Bi  $s$  and O  $p$  levels plotted in Figure 1.d. Between -12 to -6 eV, we clearly observe four bands that have a dominant Bi  $s$  character rather indicating that both  $\text{Bi}_S$  and  $\text{Bi}_L$  cations have filled  $6s$  levels. This is confirmed by our Wannier Functions (WFs) analysis based on these 4 Kohn-Sham states that yields one  $s$ -like WF per Bi cation (Figure 1.c). In contrast, we observe two bands above the Fermi level that have a dominant O  $p$  character. Building again the WF for these two bands, we obtain two  $s$ -like WF centered on  $\text{Bi}_S$  cations with large contributions coming from neighboring O anions (Figure 1.b). These two WF are in fact the two oxygen holes that are formed during the charge transfer from O to  $\text{Bi}_S$  cations. This result is in close agreement with the work of Foyevtsova *et al* and the electronic structure of  $\text{SrBiO}_3$  can be interpreted in terms of  $\text{Bi}_L 6s^2$  and  $\text{Bi}_S 6s^2\bar{L}^2$  [33] where the notation  $\bar{L}$  labels a ligand hole.

Having now established that the structural and electronic properties of  $\text{SrBiO}_3$  are in good agreement with experiments and recent theoretical works, we now turn our attention to spin-orbit related phenomena. When including the spin-orbit interaction in the calculation, we do not observe any sizable effect on the ground state properties, rather suggesting a marginal SOI in this material. However, the fact that  $\text{SrBiO}_3$  is paraelectric in its bulk hinders possible Rashba phenomena. Surprisingly, we observe the existence of a ferroelectric phonon mode at relatively low frequency ( $\omega_{\text{FE}} \simeq 50 \text{ cm}^{-1}$ ) in the bulk. Therefore, through the coupling of this phonon mode with epitaxial strain [50], one may expect to unlock ferroelectricity in  $\text{SrBiO}_3$ . This is reinforced by the ability of Bi-based oxide perovskites to exhibit ferroelectricity in bulk or under epitaxial strain. Since the pseudocubic lattice parameter of  $\text{SrBiO}_3$  is rather large ( $a_{\text{pc}} \simeq 4.26$  Å), we only explored the effect of a compressive strain in our simulations. Additionally, the SOI having marginal effect on the structural aspect of the bismuthate, we ignored it during geometry relaxation under strain.

Figure 2 reports the energy of the most stable structures found in the calculations as a function of the substrate lattice parameter (lower scale)/compressive strain value (upper scale) [51]. Between 0 and 5 % of compression,  $\text{SrBiO}_3$  remains a paraelectric insulator adopting a

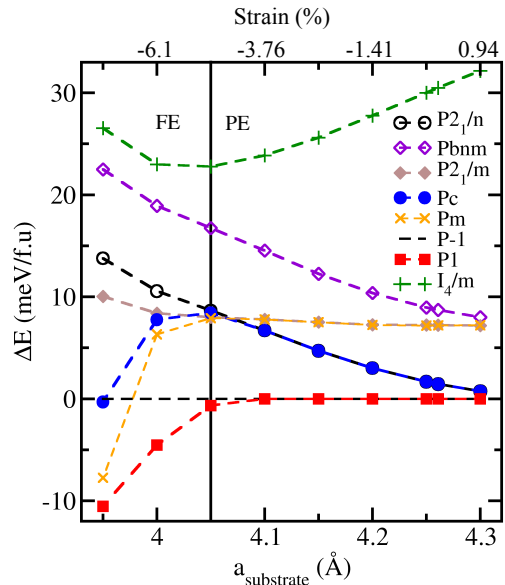


FIG. 2. Energy differences (in meV/f.u.) between the different metastable phases as a function of the substrate lattice parameter (in Å, lower scale) or strain value (in %, upper scale). The reference energy is set to the  $P-1$  structure energy (dashed horizontal black line). The vertical line represents the boundary between ferroelectric (FE) and paraelectric (PE) phases.

$P\bar{1}$  structure described by a  $a^-a^-c^+$  oxygen cage rotation patterns and a breathing of  $\text{O}_6$  groups. This structure is equivalent to the bulk except that the in-phase oxygen cage rotation axis is aligned along the substrate – such a growth is sometimes referred to  $c-P2_1/n$ , the notation  $c-$  indicating that the  $c$  axis is aligned along the substrate [52]. Beyond 5% of compression, the ground state becomes ferroelectric and is associated with a  $P1$  structure exhibiting the aforementioned structural distortions plus a spontaneous polarization in all three directions. Focusing on the structure obtained at 6.1 % of compressive strain – *i.e.*  $a_{\text{substrate}}=4$  Å–,  $\text{SrBiO}_3$  develops a polarization of  $12.65 \mu\text{C}\cdot\text{cm}^{-2}$  ( $P_x=9.64$ ,  $P_y=2.73$ ,  $P_z=-7.73$  in a pseudo  $P2_1/n$  20-atom unit cell setting,  $c$  being the long axis) approaching the value of the popular ferroelectric  $\text{BaTiO}_3$ .

When including the SOI in the ferroelectric phase, we now observe several splittings of the “oxygen hole bands” located above the Fermi level  $E_F$  (see Figure 3.a) in all reciprocal directions due to the presence of polarization along the three cartesian axes. The largest energy splitting is observed at the  $\Gamma$  point 2 eV above  $E_F$ , a smaller one being present at the bottom of the conduction band at the D point 0.70 eV above  $E_F$ . Turning our attention to bands around  $\Gamma$ , proper inspection of their spin flavors along a  $(-B)-(\Gamma)-(B)$  path (*i.e.*  $-k_x$  to  $+k_x$ ) reveals that

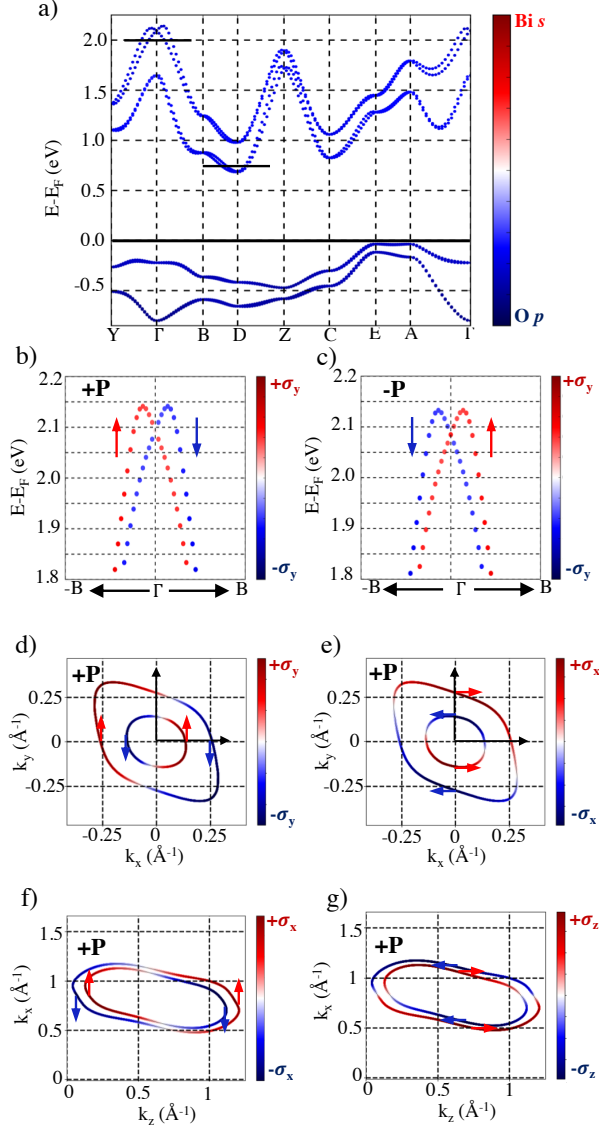


FIG. 3. Electronic properties of the ferroelectric ground state of  $\text{SrBiO}_3$  at 6.1 % of compressive strain. a) Orbital projected – on O  $p$  (blue character) and Bi  $s$  (red character) states – band structure in a monoclinic  $P2_1/n$  setting. The Fermi level is set to 0 eV. b and c) Bands projected on the  $\pm\sigma_y$  component along the  $(-1/2, 0, 0)$  to  $(+1/2, 0, 0)$  direction for +P (c) or -P (d) spontaneous polarization. d and e) Spin textures in the  $(k_x, k_y)$  plane obtained at  $E=+2$  eV when projecting on the  $\pm\sigma_y$  (d) or  $\pm\sigma_x$  (e) spin component for a positive spontaneous polarization. f) and g) Spin textures in the  $(k_z, k_x)$  plane obtained at  $E=+0.75$  eV when projecting on the  $\pm\sigma_x$  (f) or  $\pm\sigma_z$  (g) spin component for a positive spontaneous polarization.

their degeneracy is lifted according to the spin direction as illustrated by Figure 3.b. Looking at spin textures in the  $(k_x, k_y)$  plane represented in Figures 3.d and 3.e, we clearly observe two energy contours with clockwise (outer contour) and counter-clockwise (inner contour)

spin-locking of electrons with respect to their momentum following equation 1. Consequently, the ferroelectric phase of  $\text{SrBiO}_3$  reached under compressive epitaxial strain undergoes a Rashba interaction. Approximating the Rashba coefficient by  $\alpha_R = 2E_R/k_R$ , where  $E_R$  is the energy splitting of the bands with respect to the high-symmetry position and  $k_R$  is the momentum offset, we estimate an unprecedented Rashba coefficient of  $8.397 \text{ eV}\cdot\text{\AA}$  ( $E_R=48.07 \text{ meV}$ ,  $k_R=0.01145 \text{ \AA}^{-1}$ ) for the bands corresponding to the strongly hybridized electronic structure between O  $p$  and Bi  $s$  states. At the conduction band minimum, we do estimate rather large Rashba coefficients of  $0.944 \text{ eV}\cdot\text{\AA}$  and  $0.474 \text{ eV}\cdot\text{\AA}$  along the D-Z and D-B directions respectively (see Figures 3.f and g for the spin textures). Albeit smaller than values reported at the  $\Gamma$  point, these Rashba coefficients remain comparable to values observed in  $\text{BiAlO}_3$  [17] or in heavy metals such as (111) oriented Bi [26].

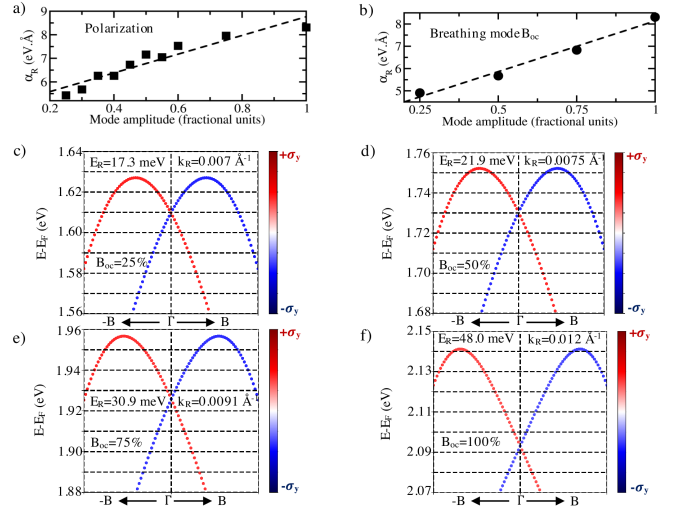


FIG. 4. Evolution of the Rashba coefficient when freezing different amplitudes of the polar distortion (a) and the breathing of the oxygen cage octahedra (b). c, d, e and f) Bands projected on the  $\pm\sigma_y$  component along the  $(-1/2, 0, 0)$  to  $(+1/2, 0, 0)$  direction for different amplitudes of the breathing distortion. We emphasize that all other lattice distortions are fixed to their amplitude appearing in the ferroelectric ground state.

We now turn our attention to possible functionalization of the Rashba interaction in this ferroelectric material. Firstly, as inferred by Figures 3.b and 3.c, switching the polarization reverses the spin textures therefore allowing their non-volatile electrical control. By freezing different amplitudes of the ferroelectric distortion while keeping other distortions to their ground state amplitude, we observe a linear dependence of  $\alpha_R$  with the ferroelectric mode amplitude (see Figure 4.a), in agreement with its dependence with the electric field amplitude. Eventually, such functionalities were already proposed theoret-

cally in GeTe [16] or in BiAlO<sub>3</sub> [17]. A key aspect of the bismuthate is the strong relationship between the breathing mode B<sub>oc</sub> and electronic properties. Although B<sub>oc</sub> is found to open the band gap in the ferroelectric phase upon its condensation in our simulations – all other lattice distortions are fixed to their ground state amplitude –, it also controls the amplitude of the Rashba coefficient as inferred by Figures 4.b, c, d, e and f. Consequently, at odds with usual assumptions, the Rashba coefficient is not only sensitive to the spin-orbit strength  $\lambda_{SO}$  and the electric field amplitude, but it can also be strongly related to structural distortions altering the band dispersions and the level of hybridization between the B site cation and O states [53]. The latter observation is in close agreement with the work of Bahramy *et al* highlighting that hybridized electronic states around  $E_F$  were a key aspect for large  $\alpha_R$  [27].

Although the ferroelectric phase is reached at relatively large compressive strain value, it might be achieved experimentally using scandate substrates for instance. Additionally, the control of the breathing mode may be unlocked by several external stimuli such as strain engineering, octahedra connectivity [54] or with hybrid improper ferroelectricity [50].

In conclusion, we have predicted in this Letter unprecedented Rashba spin splittings of oxygen hole bands in the covalent oxide perovskite SrBiO<sub>3</sub>. We have also demonstrated that the Rashba coefficient  $\alpha_R$  could be strongly related to lattice distortions irrespective of the amplitude of the electric field or of the spin-orbit interaction. The Rashba physics being at the core of the most recent spin-orbitronics based applications, our work unveils new pathways to optimize and control  $\alpha_R$  through the subtle interplay between lattice and electronic degrees of freedom appearing in oxide perovskites.

This work has been supported by the European Research Council (ERC) Consolidator grant MINT under the contract #615759. Calculations took advantages of the Occigen machines through the DARI project EPOC #A0020910084 and of the DECI resource FIONN in Ireland at ICHEC through the PRACE project FiPSCO. J. Varignon acknowledges technical help from Adam Ralph from ICHEC.

---

\* julien.varignon@cnsr-thales.fr

- [1] C. Chappert, A. Fert and F. N. VanDau, *Nat. Mater.* **6**, 813 (2007).
- [2] S. Manipatruni, D. E. Nikonov, R. Ramesh, H. Li, I. A. Young, arXiv:1512.05428v2 (2017).
- [3] M. I. D'yakonov and V. I. Perel, *JETP Letters* **13**, 467 (1971).
- [4] Y. K. Kato, R. C. Myers, A. C. Gossard and D. D. Awschalom, *Science* **306**, 1910 (2004).
- [5] H. Zhao, E. J. Loren, H. M. van Driel and A. L. Smirl, *Phys. Rev. Lett.* **96**, 246601 (2006).
- [6] K. Ando and E. Saitoh, *Nat. Commun.* **3**, 629 (2012).
- [7] L. Liu, C.-F. Pai, Y. Li, H. W. Tseng, D. C. Ralph and R. A. Buhrman, *Science* **336**, 555 (2012).
- [8] Y. A. Bychkov and E. I. Rashba, *JETP Lett.* **39**, 78 (1984).
- [9] V. M. Edelstein, *Solid State Commun.* **73**, 233 (1990).
- [10] J. C. Rojas Sánchez, L. Vila, G. Desfonds, S. Gambarelli, J.P. Attané, J. M. Teresa, C. Magén and A. Fert, *Nature Commun.* **4**, 2944 (2013).
- [11] C. R. Ast, J. Henk, A. Ernst, L. Moreschini, M. C. Falub, D. Pacilé, P. Bruno, K. Kern and M. Grioni, *Phys. Rev. Lett.* **98**, 186807 (2007).
- [12] T. Aruga, *J. Electron Spectrosc. Relat. Phenom.* **201**, 74 (2015).
- [13] K. Yaji, Y. Ohtsubo, S. Hatta, H. Okuyama, K. Miyamoto, T. Okuda, A. Kimura, H. Namatame, M. Taniguchi and T. Aruga, *Nature Commun.* **1**, 17 (2010).
- [14] E. Lesne, Y. Fu, S. Oyarzún, J.-C. Rojas-Sánchez, D. C. Vaz, H. Naganuma, G. Sicoli, J.-P. Attané, M. Jamet, E. Jacquet, J.-M. Georges, A. Barthélémy, H. Jaffres, A. Fert, M. Bibes and L. Vila, *Nat. Mater.* **15**, 261 (2016).
- [15] K. Ishizaka, M. S. Bahramy, H. Murakawa, M. Sakano, T. Shimojima, T. Sonobe, K. Koizumi, S. Shin, H. Miyahara, A. Kimura, K. Miyamoto, T. Okuda, H. Namatame, M. Taniguchi, R. Arita, N. Nagaosa, K. Kobayashi, Y. Murakami, R. Kumai, Y. Kaneko, Y. Onose and Y. Tokura, *Nat. Mater.* **10**, 521 (2011).
- [16] D. Di Sante, P. Barone, R. Bertacco and S. Picozzi, *Adv. Mater.* **25**, 509 (2013).
- [17] L. G. D. da Silveira, P. Barone and S. Picozzi, *Phys. Rev. B* **93**, 245159 (2016).
- [18] G. Dresselhaus, *Phys. Rev.* **100**, 580 (1955).
- [19] P. Zubko, S. Gariglio, M. Gabay, P. Ghosez and J.-M. Triscone, *Annu. Rev. Condens. Matter Phys.* **2**, 141 (2011).
- [20] M. L. Medarde, *J. Phys.: Condens. Matter* **9**, 1679-1707 (1997).
- [21] A. Mercy, J. Bieder, J. Iñiguez and P. Ghosez, *Nat. Commun.* **8**, 1677 (2017).
- [22] W. C. Koehler and E. O. Wollan, *J. Phys. Chem. Solids* **2**, 100 (1957).
- [23] W. C. Koehler, E. O. Wollan and M. K. Wilkinson, *Phys. Rev.* **118**, 58 (1960).
- [24] H. M. Christen, *Appl. Phys. Lett.* **88**, 262906 (2006).
- [25] Seung-Gu Lim, Stas Kriventsov and Thomas N. Jackson, *J. Appl. Phys.* **91**, 4500 (2002).
- [26] Y.M. Koroteev *et al*, *Phys. Rev. Lett.* **93**, 046403 (2004).
- [27] M. S. Bahramy, R. Arita and N. Nagaosa, *Phys. Rev. B* **84**, 041202(R) (2011).
- [28] B. J. Kennedy, C. J. Howard, K. S. Knight, Z. Zhang and Q. Zhou, *Acta Cryst. Sec. B* **62**, 537 (2006).
- [29] S. M. Kazakov *et al*, *Nature* **390**, 148 (1997).
- [30] D. E. Cox and A. W. Sleight, *Solid State Commun.* **19**, 969 (1976).
- [31] R. P. S. M. Lobo and F. Gervais, *Phys. Rev. B* **52**, 13294 (1995).
- [32] R. P. S. M. Lobo and F. Gervais, *Solid State Commun.* **98**, 61 (1996).
- [33] K. Foyevtsova, A. Khazraie, I. Elfimov, G. A. Sawatzky, *Phys. Rev. B* **91**, 121114 (2015).
- [34] T. Thonhauser and K. M. Rabe, *Phys. Rev. B* **73**, 212106 (2006).
- [35] H. Sato, S. Tajima, H. Takagi and S. Uchida, *Nature*

- 338**, 241 (1989).
- [36] A. W. Sleight, J. L. Gillson and P. E. Bierstedt, In *Ten Years of Superconductivity: 1980–1990*, pages 257–258. Springer, 1993.
  - [37] K. Ha Kim, C. U. Jung, T. W. Noh and S. C. Kim, Phys. Rev. B **55**, 15393 (1997).
  - [38] S. M. Kazakov *et al*, Nature **390**, 148 (1997).
  - [39] B. Yan, M. Jansen and C. Felser, *Nat. Phys.* **9**, 709 (2013).
  - [40] G. Kresse and J. Haffner, Phys. Rev. B **47**, 558 (1993).
  - [41] G. Kresse and J. Furthmüller, Comput. Mater. Sci. **6**, 15 (1996).
  - [42] J. P. Perdew *et al*, Phys. Rev. Lett. **100**, 136406 (2008).
  - [43] P. E. Blöchl, Phys. Rev. B **50**, 17953 (1994).
  - [44] S. Baroni, S. de Gironcoli, A. Dal Corso, P. Giannozzi, Rev. Mod. Phys. **73** (2001) 515.
  - [45] X. Gonze, C. Lee, Phys. Rev. B **55** (1997) 10355.
  - [46] A. H. Romero and F. Munoz, url = <http://sourceforge.net/p/pyprocar/PyPROCAR/HEAD/tree/> (2015).
  - [47] A. Mostofi *et al*, Comput. Phys. Commun. **178**, 685 (2008).
  - [48] N. Marzari and D. Vanderbilt, Phys. Rev. B **56**, 12847 (1997).
  - [49] I. Souza, N. Marzari and D. Vanderbilt, Phys. Rev. B **65**, 035109 (2001).
  - [50] J. Varignon, N. C. Bristowe, E. Bousquet and Ph. Ghosez, Comptes Rendus Physique **16**, 153 (2015).
  - [51] We have tested several structures combining different oxygen cage rotations pattern and/or breathing distortion  $B_{oc}$  and/or polar axes. Two growth orientation were used with either the  $a$  and  $b$  lattice parameters aligned at  $45^\circ$  of the  $a_{sub}$  and  $b_{sub}$  substrate lattice parameters or the  $c$  lattice parameter along the substrate. The eight most stable structures identified in the calculations are the following :  $P2_1/n$  ( $a^-a^-c^+ + B_{oc}$ ),  $Pc$  ( $a^-a^-c^+ + B_{oc} + P_xP_yP_z$ ),  $Pbnm$  ( $a^-a^-c^+$ ),  $P2_1/m$  ( $a^+a^-c^-$ ),  $Pm$  ( $a^+a^-c^- + P_z$ ),  $P\bar{1}$  ( $a^+a^-c^- + B_{oc}$ ) and  $P1$  ( $a^+a^-c^- + B_{oc} + P_xP_yP_z$ ).
  - [52] The  $P\bar{1}$  and  $P1$  structures grow with the in-phase rotation axis along the substrate. We therefore have to use a 40 atoms unit cell to model the constraint in our calculations. Nevertheless, results regarding band structures and polarizations are reported with respect to a 20 atoms unit cell where the  $c$  axis is the long axis of the perovskite.
  - [53] Through the condensation of the breathing distortion in the ferroelectric ground state achieved under compressive strain, the asymmetry of the sphere integrated charges between  $Bi_S$  and  $Bi_L$  increases from 0e to 0.44e, rather suggesting a strong modification of the electronic structure.
  - [54] Z. Liao *et al*, Nat. Mater. **15**, 425 (2016).